Materials Research Letters

ISSN: 2166-3831 (Online) Journal homepage: www.tandfonline.com/journals/tmrl20

In situ transformation boosts the pseudocapacitance of CuNi-MOF via cooperative orientational and electronic governing

Xianyu Chu, Fanling Meng, Wei Zhang, Lihua Zhang, Sebastian Molin, Piotr Jasinski & Weitao Zheng

To cite this article: Xianyu Chu, Fanling Meng, Wei Zhang, Lihua Zhang, Sebastian Molin, Piotr Jasinski & Weitao Zheng (2023) In situ transformation boosts the pseudocapacitance of CuNi-MOF via cooperative orientational and electronic governing, Materials Research Letters, 11:6, 446-453, DOI: 10.1080/21663831.2023.2181111

To link to this article: https://doi.org/10.1080/21663831.2023.2181111

© 2023 The Author(s). Published by Informa UK Limited, trading as Taylor & Francis Group.

View supplementary material

Published online: 28 Feb 2023.

Submit your article to this journal

Article views: 2364

View related articles

View Crossmark data

Citing articles: 23 View citing articles

Full Terms & Conditions of access and use can be found at
https://www.tandfonline.com/action/journalInformation?journalCode=tmrl20

MATER. RES. LETT.
2023, VOL. 11, NO. 6, 446–453
https://doi.org/10.1080/21663831.2023.2181111

ORIGINAL REPORTS

OPEN ACCESS

In situ transformation boosts the pseudocapacitance of CuNi-MOF via cooperative orientational and electronic governing

Xianyu Chu[a,b], Fanling Meng[a], Wei Zhang[a], Lihua Zhang[c], Sebastian Molin[d], Piotr Jasinski[d] and Weitao Zheng[a]

[a]Key Laboratory of Automobile Materials MOE, School of Materials Science & Engineering, Jilin Provincial International Cooperation Key Laboratory of High-Efficiency Clean Energy Materials, Electron Microscopy Center, International Center of Future Science, Jilin University, Changchun, People's Republic of China; [b]Key Laboratory of Preparation and Application of Environmental Friendly Materials of the Ministry of Education, Jilin Normal University, Changchun, People's Republic of China; [c]Center for Functional Nanomaterials, Brookhaven National Laboratory, Upton, NY, USA; [d]Faculty of Electronics, Telecommunications and Informatics, Gdansk University of Technology, Gdansk, Poland

ABSTRACT

The disordered arrangement and thereof inferior conductivity of 2D MOF sheets seriously hinder their practical application. Herein, we propose in situ transformation strategy to architect vertically oriented bimetallic CuNi-MOF as a self-supporting electrode, leading to a decuple high specific capacitance of 1262 C g^{-1} in comparison with the pristine Ni-MOF powder of 114 C g^{-1} at 2 A g^{-1}. DFT calculations reveal that introduction of Cu can modulate the electronic structure of metal centers in the Ni-MOF sheets and optimize electrical conductivity. Our strategy is promising to maximize the utilization of MOF superiorities for optimizing their electrochemical performance.

IMPACT STATEMENT

We provide an in situ transformation strategy for synthesizing high-activity oriented bimetallic MOFs derived from vertically oriented $Cu(OH)_2$ nanowires, with which an order of magnitude of performance-improved electrodes were produced for pseudocapacitance.

ARTICLE HISTORY
Received 8 December 2022

KEYWORDS
Metal-organic frameworks; transformation; vertically oriented; electronic configuration modification; supercapacitors

1. Introduction

Two-dimensional metal-organic frameworks (2D MOFs) have attracted wide attention for supercapacitors due to their unique structural characteristics such as large specific surface area, adjustable pore structure and composition [1–4]. Especially, under the premise of maintaining excellent power density, it can achieve high capacity and considerable energy density, compared with bulk MOFs [5–8]. It can store charge either by electrostatic absorption/desorption on the surface/subsurface through the electric double-layer energy storage mechanism or the redox reaction of metal centers [9–14]. However, the insulation properties of pools of MOFs have seriously hindered their practical application in electrochemical energy storage [15].

Although the use of carbon nanotubes [16], graphene [17–19] and other conductive carbon [20] composites is a common method to compensate for the poor conductivity of MOFs, the challenges remain as the usually random distribution affects the exposure of active sites and the relatively weak carbon/MOF interaction reduces the exploiting of MOFs. The design of integrated electrodes with an oriented structure enables a sufficient utilization of active materials and enhances the binding force with the substrate to reduce contact resistance. Another effective method is to directly synthesize conductive MOFs [21–23]. However, the cost of their preparation is quite high. Doping enables regulating carrier migration effectively and induces more electroactive sites [24,25]. Therefore, heteroatomic doping is an efficient compromise to improve the electrical conductivity and enrich the redox chemistry of materials by manipulating the electronic state of MOF electrode materials [26,27].

Herein, stimulated by the well-known in situ phase transformation phenomena, we proposed a new strategy for reversing the inferior conductivity and upgrading the electrochemical performance of MOFs by fabricating oriented bimetallic 2D MOF integrated electrodes using vertically oriented $Cu(OH)_2$ nanowires as a precursor. The $Cu(OH)_2$ acts as a structural guide agent to induce

CONTACT Wei Zhang weizhang@jlu.edu.cn Key Laboratory of Automobile Materials MOE, and School of Materials Science & Engineering, and Jilin Provincial International Cooperation Key Laboratory of High-Efficiency Clean Energy Materials, and Electron Microscopy Center, and International Center of Future Science, Jilin University, Changchun 130012, People's Republic of China

Supplemental data for this article can be accessed here. https://doi.org/10.1080/21663831.2023.2181111

© 2023 The Author(s). Published by Informa UK Limited, trading as Taylor & Francis Group.
This is an Open Access article distributed under the terms of the Creative Commons Attribution-NonCommercial License (http://creativecommons.org/licenses/by-nc/4.0/), which permits unrestricted non-commercial use, distribution, and reproduction in any medium, provided the original work is properly cited.

self-assembly of the targeting products to form oriented structures. The nickel ions in the pristine Ni-MOF crystal have been partly substituted by the isostructurally introduced Cu ions. It can not only enhance the electrode/substrate interaction and reduce the ion/electron transfer limit effectively but also accelerate the electrochemical reaction kinetics. Moreover, we reveal the regulation behavior of heterogeneous metal atoms on the electronic structure by DFT calculation. Consequently, the fabricated CuNi-MOF/CF (copper foam) electrode exhibits an order of magnitude of performance improvement due to the regularly oriented morphology and the modulated conductivity by introducing Cu^{2+} to the Ni-MOF matrix. It can achieve an ultrahigh specific capacity of 1262 C g^{-1} in comparison with the pristine Ni-MOF powder of 114 C g^{-1} at 2 A g^{-1}. Furthermore, the assembled asymmetric supercapacitor (ASC) device CuNi-MOF/CF//AC (activated carbon) has a high operated voltage window of 1.7 V, maximum energy density of 20.31 Wh kg^{-1} and maximum power density of 10,200 W kg^{-1}. This work enables fabricating the integrated MOF-based electrodes easily and efficiently with improved conductivity and enhanced electrochemical performance via in situ phase transformation strategy.

2. Materials preparation

Figure 1(a) shows the process of preparing CuNi-MOF/CF nanosheets. Firstly, $Cu(OH)_2$ nanowire precursors were in situ grown on the surface of copper foam by the surface oxidation method. Morphology characterization of $Cu(OH)_2$ based on SEM and TEM was performed (Figure S1). In an alkaline environment, the copper foam substrate is oxidized to Cu^{2+} ions via the $(NH_4)_2S_2O_8$ oxidant, and NH_3 is released in the oxidation process to form porous nanostructures. The Cu^{2+} ions trap OH^-, nucleate and grow on the copper surface, and finally obtain bright blue $Cu(OH)_2$ nanowire arrays, as follows [28,29]:

$$Cu + 4NaOH + (NH_4)_2S_2O_8 \rightarrow Cu(OH)_2 + 2Na_2SO_4 + 2NH_3 \uparrow + 2H_2O$$

Secondly, $Cu(OH)_2$/CF was placed as a template and precursor in a mixed solution containing terephthalic acid and nickel chloride, and held at 120°C for 24 h to generate light green CuNi-MOF nanosheets. The synthesis process can be explained by the mechanism of solution recrystallization. $Cu(OH)_2$ is an amphoteric hydroxide that reacts with PTA molecules since one PTA molecule has two carboxylic groups. In the presence of $NiCl_2 \cdot 6H_2O$, CuNi-MOF nanosheets were successfully

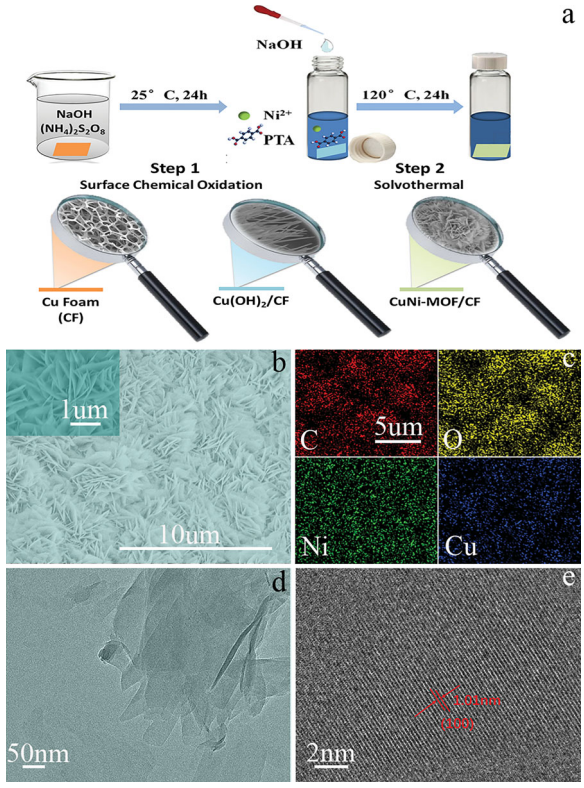

Figure 1. (a) Schematic diagram of the preparation of CuNi-MOF/CF, (b) SEM image with a local enlargement, (c) EDS elemental maps, (d) TEM and (e) HRTEM images of CuNi-MOF.

synthesized with the following reaction:

$$(3-x)Ni^{2+} + xCu^{2+} + 2(C_8H_4O_4)^{2-} + 2OH^- + 6H_2O \rightarrow [Ni_{3-x}Cu_x(OH)_2(C_8H_4O_4)_2 \cdot (H_2O)_4] \cdot 2H_2O$$

Compared with the coating method, the in situ growth strategy has obvious advantages (Supporting Information).

3. Results and discussion

The CuNi-MOF nanosheets with a thickness of ~100 nm are uniformly covered on the copper foam (Figure 1(b)). The oriented nanosheet structure can significantly increase the effective specific surface area that is accessible to the electrolyte ions, improve the reaction kinetics, and expose more reaction sites toward higher electrode capacity. C, O, Ni, and Cu are well distributed in CuNi-MOF (Figure 1(c)). The atomic ratio of Cu:Ni is ~1:10 (Figure S2). Therefore, the contribution to capacitance is mainly controlled by nickel. The dispersed and interlaced nanosheets were further confirmed by SEM (Figure 1(b)) and TEM images (Figure 1(d)). The typical (100) crystal plane of CuNi-MOF was identified by

HRTEM (Figure 1(e)). For the layered structure of CuNi-MOF, the maximum exposure surface enables facilitating both electron transport and ion diffusion.

All the main XRD peaks are indexed as $Cu(OH)_2$ (JCPDS no. 13-0420) [30] except for the copper foam substrate marked by an asterisk (Figure 2(a)). The XRD pattern of CuNi-MOF is similar to that of the Ni-MOF powder synthesized by the same method without the addition of $Cu(OH)_2$/CF precursor, in agreement with the simulated pattern of $[Ni_3(OH)_2(C_8H_4O_4)_2.(H_2O)_4].2H_2O$ (CCDC no. 638866) [31], indicating that nickel ions have been partly substituted by copper ions in the pristine Ni-MOF crystal. Considering the disappearance of the diffraction peak of $Cu(OH)_2$, the $Cu(OH)_2$ precursor was successfully transformed into CuNi-MOF. Figure 2(b) shows the FT-IR spectra of $Cu(OH)_2$, Ni-MOF and CuNi-MOF in the range of 4000–500 cm^{-1}. For $Cu(OH)_2$, the absorption peak at 3566, 3295 cm^{-1} reflects OH^- vibration and 688 cm^{-1} can be attributed to Cu–O [30], respectively. For Ni-MOF, the two absorption bands at 3607 and 3548 cm^{-1} are caused by O–H vibrations associated with hydroxyl groups and crystal water [32,33]. For CuNi-MOF, the two strong absorption zones at 1362, 1582 cm^{-1} belong to the COO stretching mode, and $\sim$820 cm^{-1} is caused by the bending vibration outside the plane of C = C–H in the benzene ring. In addition, the characteristic peaks of $Cu(OH)_2$ disappeared, confirming again that $Cu(OH)_2$ was completely transformed into CuNi-MOF. The crystal structures and molecular vibration information were further confirmed by Raman (Figure S3). Interestingly, similar Raman spectra of Ni-MOF and CuNi-MOF further confirm the isostructural phenomenon [33] consistent with the XRD analysis. In other words, $Cu(OH)_2$ not only induces the oriented growth of MOFs but also provides a copper source and participates in the formation of CuNi-MOF which is isomorphic to Ni-MOF. To analyze the elemental composition of the surface and chemical bonding states of the CuNi-MOF, X-ray photoelectron spectroscopy (XPS) was carried out to demonstrate the coexistence of Ni, Cu, O, and C elements (Figure 2(c)). Compared with Ni-MOF, the Cu 2p spectra (Figure 2(d)) can be clearly detected in CuNi-MOF, which further verifies the successful incorporation of Cu atom into Ni-MOF. The Cu 2p peaks located at 933.7 and 954.2 eV correspond to the Cu $2p_{3/2}$ and Cu $2p_{1/2}$ peaks of Cu^{2+}, respectively [34]. The intensity of the weak peak also indicates low content of Cu. The binding energy of Ni 2p at 856.4 and 874.1 eV is attributed to Ni^{2+} [35] (Figure 2(e)). The peaks at 284.6, 285.6 and 288.5 eV in C 1s corresponded to C–C/C = C, C–O and O–C = O functionalities (Figure 2(f)) [36], respectively, proving the existence of PTA in the structure.

The electrochemical performance is tested in the form of three electrodes. Figure 3(a) shows the cyclic voltammetry (CV) curves of $Cu(OH)_2$/CF, Ni-MOF and CuNi-MOF/CF electrodes at -0.2–0.7 V. Specifically, a pair of redox peaks appear in $Cu(OH)_2$/CF (Figure S4) and Ni-MOF (Figure S5), which are attributed to the Faraday reaction between Cu^+/Cu^{2+} and Ni^{2+}/Ni^{3+}, respectively. The CV curves adopt the combined action of the aforementioned two conditions for CuNi-MOF/CF. The highest current response and the largest area surrounded by the CV curve reveal improved reactivity and higher specific capacitance. The specific capacitances of $Cu(OH)_2$/CF, Ni-MOF and CuNi-MOF/CF electrodes of galvanostatic charge–discharge (GCD) at 2 A g^{-1} (Figure 3(b)) are 36, 114 and 1262 C g^{-1}, respectively, which further confirmed the feasibility and superiority of our design. The contribution to the capacitance of CuNi-MOF/CF mainly comes from nickel by controlling experiment of response current of Ni-MOF and $Cu(OH)_2$/CF. Besides, with the increase of scanning rate, the CV curve maintained its original shape and increased peak current (Figure 3(c)), i.e. its rapid current response. The charge–discharge curves show a distinct platform representing battery-type behavior, which is consistent with the CV curve [37]. The gravimetric specific capacity of CuNi-MOF electrode was further tested and delivered 1262, 1012, 864, 760, 700 and 512 C g^{-1} at current densities of 2, 4, 6, 8, 10 and 16 A g^{-1}, respectively, superior to $Cu(OH)_2$ and Ni-MOF electrodes (Figure 3(d/e)). The areal specific capacity of CuNi-MOF/CF can reach 3.9 C cm^{-2}, and Ni-MOF has only a tenth of that (0.38 C cm^{-2}) at 2 A g^{-1} (Table S1). Moreover, the electrochemical properties of the prepared CuNi-MOF electrode also have significant competitive advantages compared with other reported MOF-based electrode materials (Table S2). The charge transfer kinetics of electrode/electrolyte interface and the diffusion of electrolyte were analyzed by EIS. Each Nyquist diagram consists of a semicircle of the high-frequency region and a straight line of the low-frequency region (Figures 3(f) and S6) [38]. According to Table S3, the values of the internal resistance (R_s, 0.88 Ω) and the charge transfer resistance (R_{ct}, 0.29 Ω) of the CuNi-MOF electrode are lower than those of Ni-MOF (R_s = 1.42 Ω, R_{ct} = 32.63 Ω), indicating that copper doping can significantly improve the conductivity of the Ni-MOF material and reduce the ion/electron transfer limit. Figure S7 displays the Bode plots of CuNi-MOF/CF and Ni-MOF. At the phase angle of −45°, the time constant($\tau_0 = 1/f_0$) of CuNi-MOF/CF is 0.27 s, and it is 16.67 s for Ni-MOF, revealing that the former has a faster frequency response. From Figure 3(g), the σ values of CuNi-MOF and Ni-MOF electrodes are 0.54 and 5.95, respectively. That is,

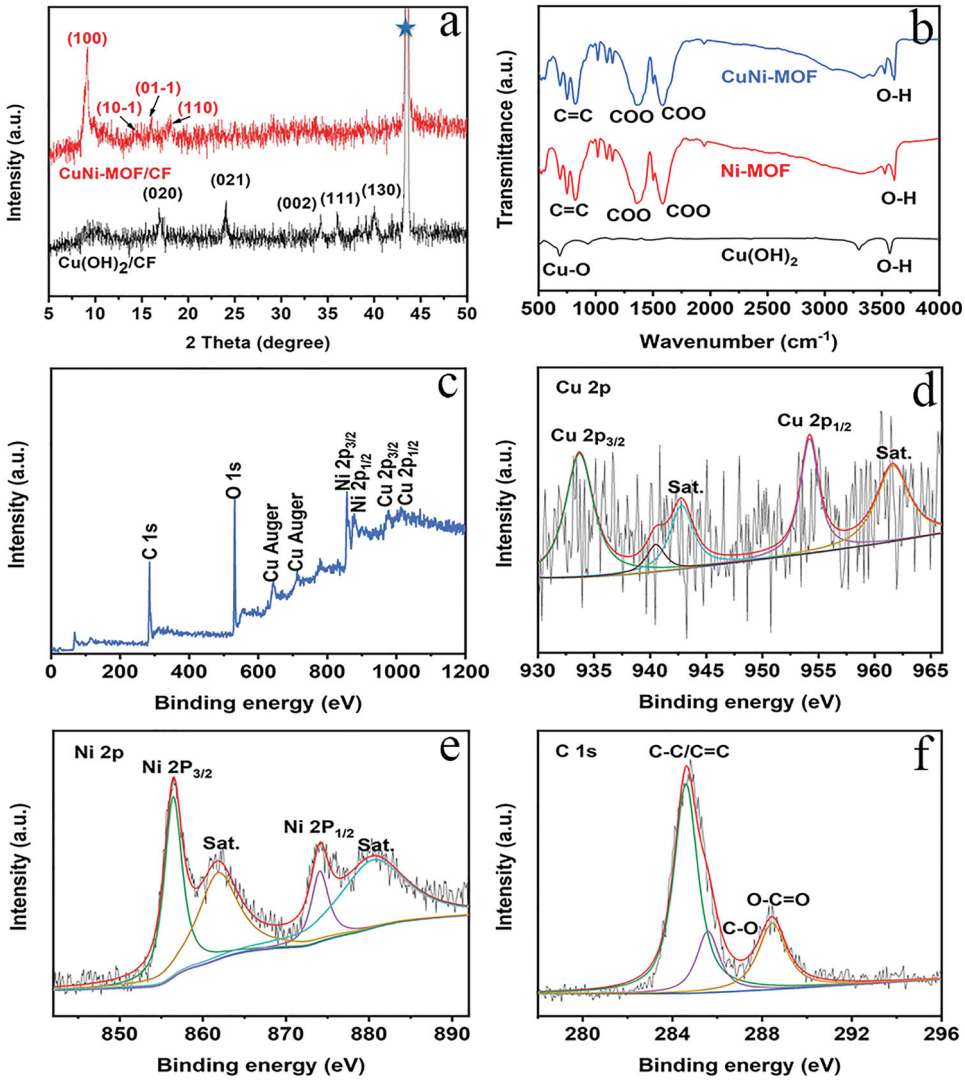

Figure 2. (a) XRD patterns of $Cu(OH)_2$/CF and CuNi-MOF/CF, (b) FT-IR spectra of $Cu(OH)_2$/CF, Ni-MOF and CuNi-MOF/CF, (c) XPS survey spectrum, (d) XPS Cu 2p spectrum, (e) XPS Ni 2p spectrum and (f) XPS C 1s spectrum of CuNi-MOF/CF.

the diffusion rate of OH^- in CuNi-MOF is higher than that of Ni-MOF. The power law rule ($i = av^b$) between peak current (i) and scanning rate (v) based on the CV curve reveals the charge storage mechanism and reaction kinetics of the electrode [39]. The b values can be determined by the slope of linear log(i)–log(v), where b values of 0.5 and 1 represent the diffusion control behavior and capacitance control behavior of the electrode material in the energy storage process, respectively [40]. The corresponding b values of the anode/cathode peak and cathode peak of the CuNi-MOF electrode are 0.52 and 0.5, respectively (Figure 3(h)), i.e. the charge storage mechanism is dominated by the diffusion control process. The coulomb efficiency of the CuNi-MOF/CF is above 93% and the excellent capacitance retention rate of the CuNi-MOF/CF electrode can still reach 82.97%, compared with the initial specific capacitance after 3000 cycles at 2 A g^{-1} (Figure 3(i)). After the stability test, the CuNi-MOF/CF still maintains the oriented nanosheet morphology (Figure S8), which indicates the structure of CuNi-MOF/CF is very stable.

In order to understand the effect of copper doping on the electrochemical performance of MOFs, density function theory (DFT) calculations were conducted. The structure models of Ni-MOF and CuNi-MOF are listed in Figure S9. To clarify the electronic structure of CuNi-MOF, the charge density difference was simulated. From Figure 4(a), there is overt electron accumulation around Ni and electron depletion around Cu, revealing charge interaction between Cu and Ni. The calculation band gap of NiCu-MOF is 0.50 eV while it is 0.86 eV for Ni-MOF by density of states (DOS). It suggests that the introduction of Cu changes the electronic structure, which improves electrical conductivity. Therefore,

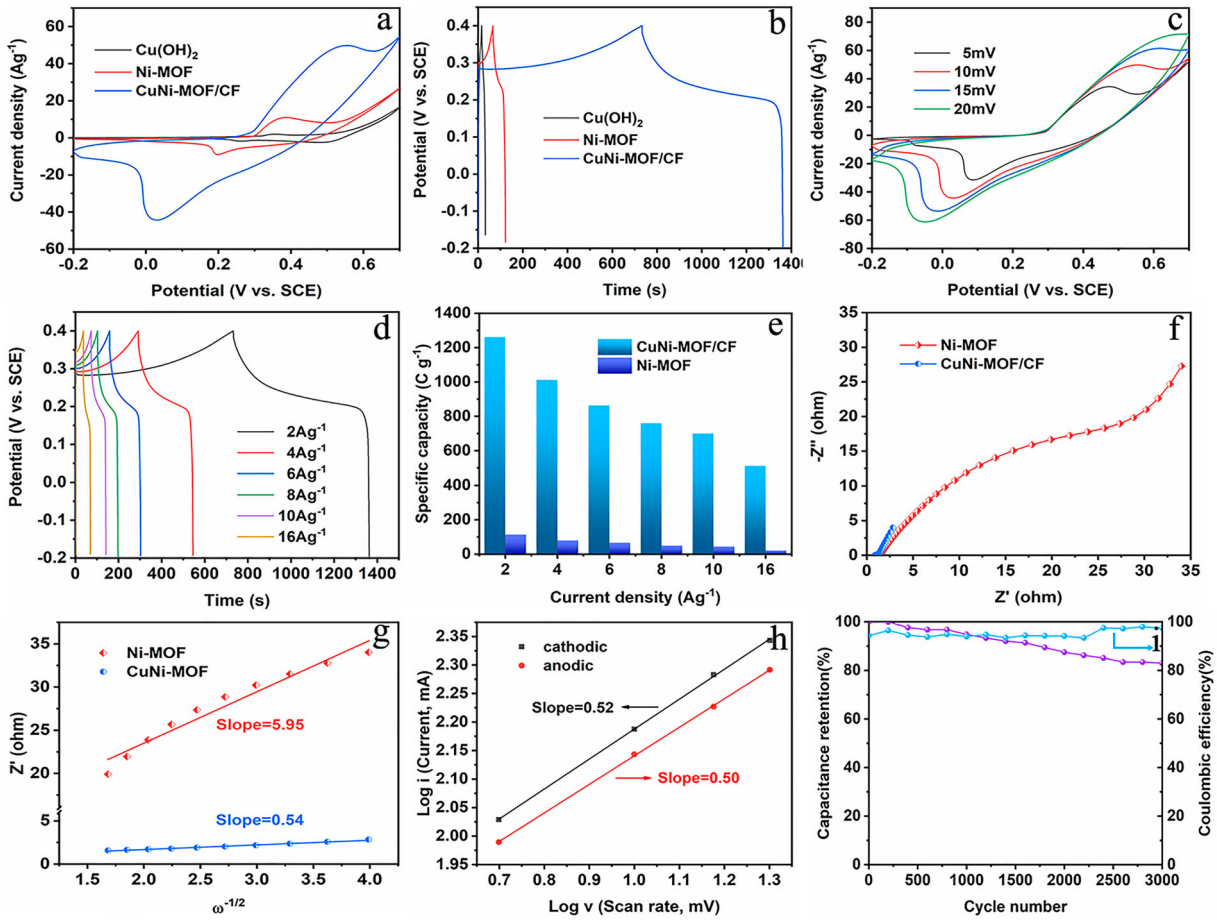

Figure 3. (a) CV curves at 10 mV s^{-1} and (b) GCD curves at 2 A g^{-1} of $Cu(OH)_2$, Ni-MOF and CuNi-MOF, (c) CV curves at different scan rates and (d) GCD curves at different current densities of CuNi-MOF, (e) the specific capacity values, (f) comparison of Nyquist plots and (g) Z′ plots against $\omega^{-1/2}$ at the low-frequency region of EIS of the Ni-MOF and CuNi-MOF, (h) *b* value and (i) coulombic efficiency and stability performance at 2 A g^{-1} of CuNi-MOF.

copper doping can significantly enhance the conductivity of Ni-MOF materials and promote charge transfer efficiency, consistent with the experiment results.

The CuNi-MOF/CF electrode has such excellent electrochemical performance, reasonably due to the following aspects: (1) The dispersed and interlaced nanosheets with amounts of open spaces are conducive to electrolyte infiltration. They shorten the ion diffusion distance, expose more active sites, promote the transfer of electrolyte/ion diffusion, and thus reverse the sluggish surface reaction kinetics; (2) the in situ transformation results in good adhesion of electrode/substrate, which effectively avoids the electrode peeling off; (3) the introduction of copper ions can effectively improve the conductivity of the original Ni-MOF, which is conducive to the efficient and rapid transmission of electrons. In addition, the synergistic interaction of Cu/Ni ions is conducive to the activation of the electrochemical reactivity of the electrode material, thus providing a high capacity.

On the aforementioned exploration, an asymmetric supercapacitor is fabricated by using the CuNi-MOF/CF and AC as the cathode and anode, respectively. Figure S10 shows the electrochemical characterization of the AC electrode, from which one can see that AC possesses good electric double- layer capacitance characteristics (Supporting information). Figure 5(a) shows the CV curves with 1.7 V operable voltage window. The CV curve is free of obvious deformation at different scanning rates from 5 to 40 mV s^{-1}, demonstrating that the capacitor has excellent rate capability. The curve is neither ideally rectangular nor obvious redox peak, i.e. the total capacitance is provided by both the CuNi-MOF /CF electrode and AC electrode. Figure 5(b) shows the GCD curves of CuNi-MOF/CF//AC. The symmetrical shape of all GCD curves illustrates that the charge storage is well balanced. As shown in Figure 5(c), the device exhibits a maximum energy density of 20.31 Wh kg^{-1} and a maximum power density of 10,200 W kg^{-1}, significantly superior to those previous devices (Table S4). Furthermore,

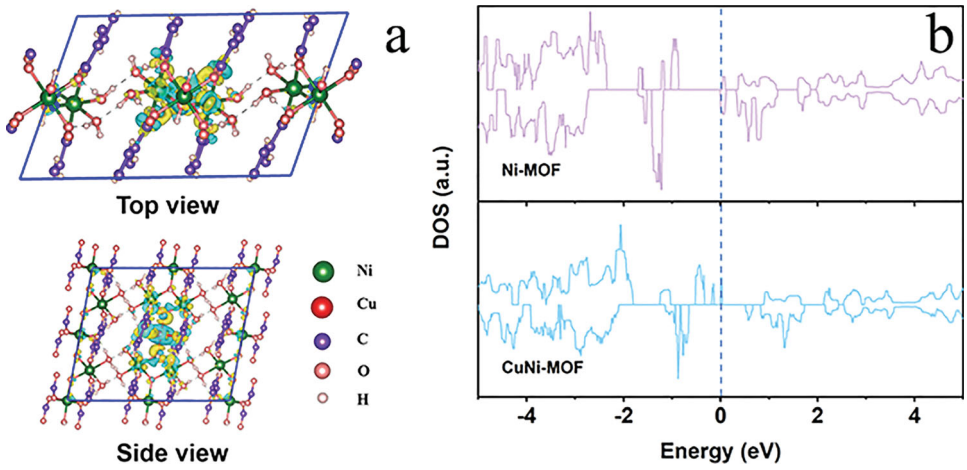

Figure 4. DFT calculation. (a) The charge density difference between Ni-MOF and CuNi-MOF, where the yellow region represents electron accumulation and the cyan region represents electron depletion. (b) DOS of Ni-MOF and CuNi-MOF.

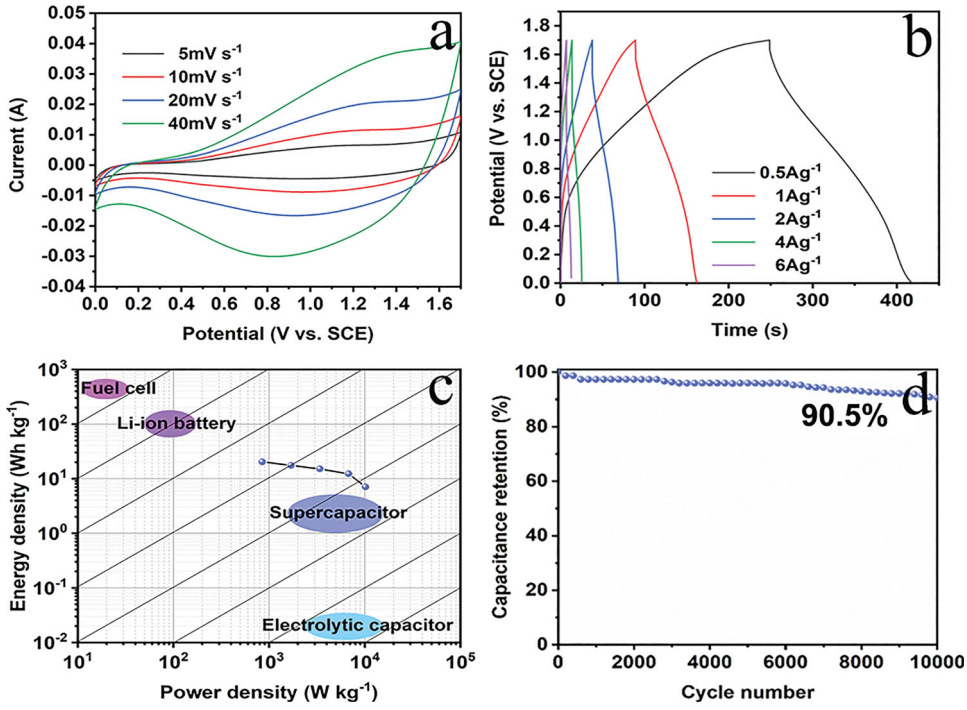

Figure 5. (a) CV, (b) GCD, (c) Ragone plot and (d) cycling performance of the CuNi-MOF/CF //AC device in 1 M KOH.

a remarkable stability performance (Figure 4(d)) shows only 9.5% decay after 10,000 cycles at $2\,A\,g^{-1}$. Thus, our design strategy is promising for tapping the application potential of MOF materials toward electrochemical energy storage.

4. Conclusions

An in situ phase transformation strategy proposed to design oriented CuNi-MOF with an order of magnitude improved electrochemical performance. The main merit lies in using vertically oriented $Cu(OH)_2$ nanowire as the precursor, where $Cu(OH)_2$ not only provides a copper source but also induces the oriented growth of the CuNi-MOF. The introduction of copper improves conductivity effectively and enhances the electrochemical performance of 2D MOFs as well. In addition, the as-fabricated CuNi-MOF/CF//AC device shows high energy density and outstanding stability performance. This work may pave the way for obtaining oriented electrode materials with excellent electrochemical performance through in situ conversion between template and target MOF products.

Disclosure statement

No potential conflict of interest was reported by the author(s).

Funding

This research is supported by the National Natural Science Foundation of China (grant numbers 52272209, 51932003, 51872115); and 2020 International Cooperation Project of the Department of Science and Technology of Jilin Province (grant number 20200801001GH). The authors express their sincere thanks to Zhenzhen Zhao and Xinyan Zhou for stimulating discussion and assistance.

ORCID

Wei Zhang http://orcid.org/0000-0002-6414-7015

References

[1] Shahrokhian S, Ezzati M, Hosseini H. Fabrication of a sensitive and fast response electrochemical glucose sensing platform based on co-based metal-organic frameworks obtained from rapid in situ conversion of electrodeposited cobalt hydroxide intermediates. Talanta. 2020;210:120696.

[2] Azadfalah M, Sedghi A, Hosseini H, et al. Cobalt based metal organic framework/graphene nanocomposite as high performance battery-type electrode materials for asymmetric Supercapacitors. J Energy Storage. 2021;33:101925.

[3] Shahrokhian S, Khaki Sanati E, Hosseini H. Direct growth of metal-organic frameworks thin film arrays on glassy carbon electrode based on rapid conversion step mediated by copper clusters and hydroxide nanotubes for fabrication of a high performance non-enzymatic glucose sensing platform. Biosens Bioelectron. 2018;112:100–107.

[4] Hosseini H, Ahmar H, Dehghani A, et al. A novel electrochemical sensor based on metal-organic framework for electro-catalytic oxidation of L-cysteine. Biosens Bioelectron. 2013;42:426–429.

[5] Ramachandran R, Zhao C, Luo D, et al. Morphology-dependent electrochemical properties of cobalt-based metal organic frameworks for supercapacitor electrode materials. Electrochim Acta. 2018;267:170–180.

[6] Zhao K, Liu S, Ye G, et al. High-yield bottom-up synthesis of 2D metal–organic frameworks and their derived ultrathin carbon nanosheets for energy storage. J Mater Chem A. 2018;6(5):2166–2175.

[7] Zhao Y, Song Z, Li X, et al. Metal organic frameworks for energy storage and conversion. Energy Storage Mater. 2016;2:35–62.

[8] Zhao Z, Zhang W, Liu M, et al. Switching optimally-balanced Fe-N interaction enables extremely stable energy storage. Energy Environ Mater. 2022. doi:10.1002/eem2.12342.

[9] Cao X, Tan C, Sindoro M, et al. Hybrid micro-/nano-structures derived from metal-organic frameworks: preparation and applications in energy storage and conversion. Chem Soc Rev. 2017;46(10):2660–2677.

[10] Gadipelli S, Li Z, Lu Y, et al. Size-related electrochemical performance in active carbon nanostructures: a MOFs-derived carbons case study. Adv Sci. 2019;6:1901517.

[11] Feng D, Lei T, Lukatskaya MR, et al. Robust and conductive two-dimensional metal—organic frameworks with exceptionally high volumetric and areal capacitance. Nat Energy. 2018;3(1):30–36.

[12] Dong T, Yi W, Deng T, et al. Diffusionless-like transformation unlocks pseudocapacitance with bulk utilization: reinventing Fe_2O_3 in alkaline electrolyte. Energy Environ Mater. 2023;6:e12262.

[13] Stoller MD, Ruoff RS. Best practice methods for determining an electrode material's performance for ultracapacitors. Energy Environ Sci. 2010;3(9):1294–1301.

[14] Liu S, Kang L, Zhang J, et al. Structural engineering and surface modification of MOF-derived cobalt-based hybrid nanosheets for flexible solid-state supercapacitors. Energy Storage Mater. 2020;32:167–177.

[15] Chu X, Meng F, Yang H, et al. Cu-doped layered double hydroxide constructs the performance-enhanced supercapacitor Via band Gap reduction and defect triggering. ACS Appl Energy Mater. 2022;5(2):2192–2201.

[16] Wen P, Gong P, Sun J, et al. Design and synthesis of Ni-MOF/CNT composites and rGO/carbon nitride composites for an asymmetric supercapacitor with high energy and power density. J Mater Chem A. 2015;3(26):13874–13883.

[17] Gupta AK, Saraf M, Bharadwaj PK, et al. Dual functionalized CuMOF-based composite for high-performance supercapacitors. Inorg Chem. 2019;58(15):9844–9854.

[18] Azadfalah M, Sedghi A, Hosseini H. Synthesis of nanoflower metal–organic framework/graphene composites As a high-performance electrode material for supercapacitors. J Electron Mater. 2019;48(11):7011–7024.

[19] Azadfalah M, Sedghi A, Hosseini H. Synergistic effect of Ni-based metal organic framework with graphene for enhanced electrochemical performance of supercapacitors. J Mater Sci: Mater Electron. 2019;30(13):12351–12363.

[20] Dahal B, Mukhiya T, Ojha GP, et al. In-built fabrication of MOF assimilated B/N co-doped 3D porous carbon nanofiber network as a binder-free electrode for supercapacitors. Electrochim Acta. 2019;301:209–219.

[21] Nam KW, Park SS, dos Reis R, et al. Conductive 2D metal-organic framework for high-performance cathodes in aqueous rechargeable zinc batteries. Nature Commun. 2019;10(1):4948.

[22] Sheberla D, Bachman JC, Elias JS, et al. Conductive MOF electrodes for stable supercapacitors with high areal capacitance. Nat Mater. 2017;16(2):220–224.

[23] Li W-H, Ding K, Tian H-R, et al. Conductive metal-organic framework nanowire array electrodes for high-performance solid-state supercapacitors. Adv Funct Mater. 2017;27(27):1702067.

[24] Liu S, Kang L, Hu J, et al. Unlocking the potential of oxygen-deficient copper-doped Co_3O_4 nanocrystals confined in carbon as an advanced electrode for flexible solid-state supercapacitors. ACS Energy Lett. 2021;6(9):3011–3019.

[25] Ezzati M, Shahrokhian S, Hosseini H. In situ Two-step preparation of 3D NiCo-BTC MOFs on a glassy carbon electrode and a graphitic screen printed electrode as nonenzymatic glucose-sensing platforms. ACS Sustainable Chem Eng. 2020;8(38):14340–14352.

[26] Zheng D, Wen H, Sun X, et al. Ultrathin Mn doped Ni-MOF nanosheet array for highly capacitive and stable asymmetric supercapacitor. Chemistry—A Eur J. 2020;26(71):17149–17155.
[27] Jiao Y, Pei J, Chen D, et al. Mixed-metallic MOF based electrode materials for high performance hybrid supercapacitors. J Mater Chem A. 2017;5(3):1094–1102.
[28] Zhu D, Yan M, Chen R, et al. 3D cu$(OH)_2$ nanowires/carbon cloth for flexible supercapacitors with outstanding cycle stability. Chem Eng J. 2019;371:348–355.
[29] Chen F, Chen C, Hu Q, et al. Synthesis of CuO@CoNi LDH on Cu foam for high-performance supercapacitors. Chem Eng J. 2020;401:126145.
[30] Patil SL, Raut SS, Sankapal BR. $Cu(OH)_2$@$Cd(OH)_2$ core-shell nanostructure: synthesis to supercapacitor application. Thin Solid Films. 2019;692:137584.
[31] Deng T, Shi X, Zhang W, et al. Unlocking the potential of metal organic frameworks for synergized specific and areal capacitances via orientation regulation. Nanotechnology. 2021;32(7):075402.
[32] Xu F, Chen N, Fan Z, et al. Ni/Co-based metal organic frameworks rapidly synthesized in ambient environment for high energy and power hybrid supercapacitors. Appl Surf Sci. 2020;528:146920.
[33] Zhang J, Wang Z, Deng T, et al. $Ni(OH)_2$ derived Ni-MOF supported on carbon nanowalls for supercapacitors. Nanotechnology. 2021;32(19):195404.
[34] Zhu S, Wang Z, Huang F, et al. Hierarchical $Cu(OH)_2$@$Ni_2(OH)_2CO_3$ core/shell nanowire arrays in situ grown on three-dimensional copper foam for high-performance solid-state supercapacitors. J Mater Chem A. 2017;5(20):9960–9969.
[35] Chu X, Meng F, Deng T, et al. Mechanistic insight into bimetallic CoNi-MOF arrays with enhanced performance for supercapacitors. Nanoscale. 2020;12(9):5669–5677.
[36] Yang C, Li X, Yu L, et al. A new promising Ni-MOF superstructure for high-performance supercapacitors. Chem Commun (Camb). 2020;56(12):1803–1806.
[37] Brousse T, Bélanger D, Long JW. To be or not to be pseudocapacitive? J Electrochem Soc. 2015;162(5):A5185–A5189.
[38] Li C, Xi Z, Dong S, et al. CNTs/MOFs-derived carbon/$Al_2(OH)_{2.76}F_{3.24}$/S cathodes for high-performance lithium-sulfur batteries. Energy Storage Mater. 2018;12:341–351.
[39] Xu X, Liu J, Liu J, et al. A general metal-organic framework (MOF)-derived selenidation strategy for in situ carbon-encapsulated metal Selenides as high-rate anodes for Na-Ion batteries. Adv Funct Mater. 2018;28(16):1707573.
[40] Huang C, Wang D, Zhang W, et al. Substitution-triggered broken symmetry of cobalt tungstate boosts redox kinetics in pseudocapacitive storage. Cell Rep Phys Sci. 2022;3(11):101115.